JACS
JOURNAL OF THE AMERICAN CHEMICAL SOCIETY

pubs.acs.org/JACS

Communication

NMR Based SARS-CoV-2 Antibody Screening

Marta V. Schoenle, Yang Li, Meng Yuan, Michael W. Clarkson, Ian A. Wilson, Wolfgang Peti,* and Rebecca Page*

Cite This: J. Am. Chem. Soc. 2021, 143, 7930−7934

Read Online

ACCESS | Metrics & More | Article Recommendations | Supporting Information

ABSTRACT: The severe acute respiratory syndrome coronavirus 2 (SARS-CoV-2) entry into cells is a complex process that involves (1) recognition of the host entry receptor, angiotensin-converting enzyme 2 (ACE2), by the SARS-CoV-2 spike protein receptor binding domain (RBD), and (2) the subsequent fusion of the viral and cell membranes. Our long-term immune-defense is the production of antibodies (Abs) that recognize the SARS-CoV-2 RBD and successfully block viral infection. Thus, to understand immunity against SARS-CoV-2, a comprehensive molecular understanding of how human SARS-CoV-2 Abs recognize the RBD is needed. Here, we report the sequence-specific backbone assignment of the SARS-CoV-2 RBD and, furthermore, demonstrate that biomolecular NMR spectroscopy chemical shift perturbation (CSP) mapping successfully and rapidly identifies the molecular epitopes of RBD-specific mAbs. By incorporating NMR-based CSP mapping with other molecular techniques to define RBD-mAb interactions and then correlating these data with neutralization efficacy, structure-based approaches for developing improved vaccines and COVID-19 mAb-based therapies will be greatly accelerated.

Coronavirus disease 2019 (COVID-19) is an ongoing global pandemic caused by the severe acute respiratory syndrome coronavirus-2 (SARS-CoV-2) ssRNA virus. Although a number of vaccines are now available to prevent serious disease and hospitalization,[1] additional treatment options, such as antivirals, anti-inflammatories, and monoclonal antibody (mAb) therapies, are desperately needed for critically ill patients battling the infection. Further, the emergence of escape variants portend the need for new or modified vaccines to combat novel variants.[2−4]

It is now well-established that many neutralizing antibodies isolated from convalescent patients target the SARS-CoV-2 spike, or 'S', protein.[5,6] The S protein is a transmembrane glycoprotein that forms homotrimers on the SARS-CoV-2 surface and mediates host cell entry and fusion via binding to the angiotensin-converting enzyme 2 (ACE2).[7−9] The S protein receptor binding domain (RBD) of the spike protein interacts with ACE2.[9] Of the 2076 SARS-CoV-2 targeting mAbs isolated since May 2020, 55% (1150) target the RBD. Furthermore, 51% of these (585) are reported as neutralizing, demonstrating the central importance of RBD for eliciting potent and effective immune responses.[10]

Defining the molecular basis of mAb recognition of the RBD provides key insights into antigenicity and sites of vulnerability, providing key molecular information to improve existing COVID-19 therapies and vaccines.[11−14] To date, 116 RBD-mAb structures have been determined using either X-ray crystallography and/or cryoelectron microscopy (cryo-EM).[10] These data have led to the discovery of three key, distinct RBD epitopes: the receptor binding site (RBS; with 4 subepitopes), the CR3022 binding site, and the S309 binding site (Figures 1A, S1, green, orange, and lavender surfaces, respectively; CR3022 and S309 are anti-RBD mAbs).[12,15,16] However, if and how these major RBD epitopes are subdivided into distinct classes of subepitopes that correlate with neutralization efficacy is an important, actively researched question. This is because the 116 mAb:RBD structures represent only a fraction (10%) of the isolated mAbs demonstrated to bind the RBD. Despite the critical insights into the mechanisms of SARS-CoV-2 neutralization provided by these structures, an additional complementary experimental method that is fast and provides molecular data regarding the mAb-RBD binding mechanism would greatly augment and accelerate these efforts.

Here, we show that biomolecular NMR chemical shift perturbation (CSP) mapping using (^{2}H,^{15}N)-labeled RBD titrated with RBD-binding Fab fragments (antibody binding fragment of mAb) can help fill this missing knowledge gap. Our data demonstrate that despite the size of the Fab-RBD complex (~70 kDa), the 2D [^{1}H,^{15}N] TROSY spectra of the RBD:RBD-binding Fab complex are of outstanding quality, allowing the CSPs to be readily analyzed and the RBD residues that mediate mAb binding to be identified. Further, because it is a solution-based technique, multiple mapping experiments can be performed in a timely manner, limited only by the time it takes to express and purify the Fabs themselves. By using NMR CSP mapping in addition to X-ray crystallography and cryo-EM, the full catalog of RBD epitopes may be molecularly defined, and not just those amenable to crystallographic and/or cryo-EM methodologies. This approach will allow the full collection of epitope-binding mAbs to be classified based on their RBD-binding interface.[12,15,16] Further, correlating neu-

Received: April 14, 2021
Published: May 21, 2021

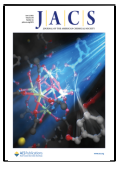

https://doi.org/10.1021/jacs.1c03945
J. Am. Chem. Soc. 2021, 143, 7930−7934

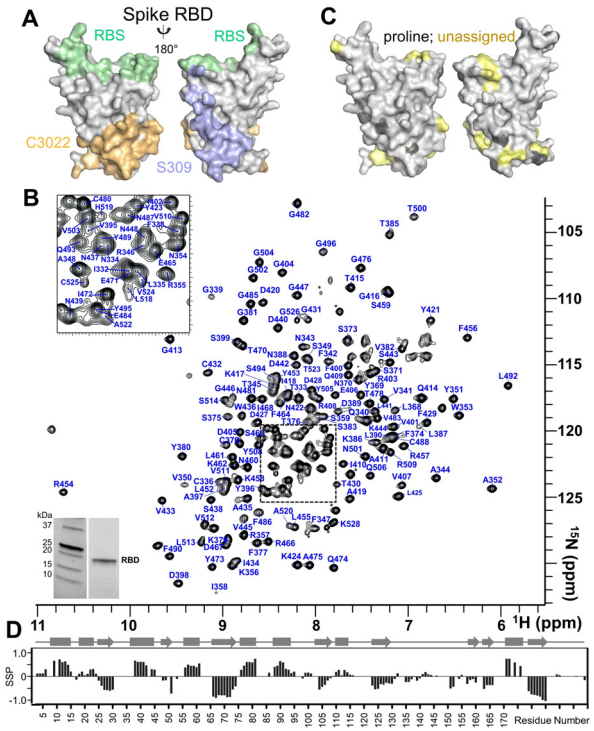

Figure 1. Sequence-specific backbone assignment of the SARS-CoV-2 spike receptor binding domain (RBD). (A) Surface representation of the RBD, with the major known antibody-binding epitopes colored in light green (receptor binding site, RBS), light orange (CR3022 binding site), and lavender (S309 binding site). (B) Fully annotated 2D [^{1}H,^{15}N] TROSY spectrum of the RBD (800 MHz ^{1}H Larmor). Assigned peaks are labeled with the corresponding residue (single letter code) and number in the protein sequence. (C) Surface representation of assigned residues. Prolines are shaded dark gray, and unassigned residues are shaded light yellow. (D) Chemical shift index/secondary structure propensity plot of the RBD; secondary structural elements are shown above.

tralization efficacy with each RBD-binding class, as has been initiated for those binding classes identified by crystallography and cryoEM,[16] will lead to novel approaches for developing improved vaccines and COVID-19 mAb-based therapies.

Fab:RBD interactions are typically strong (K_D, nM range).[11] Thus, these complexes will behave akin to an ∼70 kDa protein, which requires strict protein deuteration and the use of transverse relaxation optimized spectroscopy (TROSY).[17] Uniformly (^{2}H,^{15}N)- or (^{2}H,^{15}N,^{13}C)-labeled SARS-CoV-2 RBD (aa 331−528) was expressed as inclusion bodies in *E. coli* and the protein refolded by rapid dilution using a reduced-oxidized glutathione (GSH:GSSG) redox buffer (Figure 1B, inset). Properly folded RBD was isolated using size exclusion chromatography, and the thermal stability, T_m, was determined to be 49.6 ± 0.1 °C (SEM; n = 4).

Because CSP mapping experiments are only capable of defining protein:protein interactions with a highly complete specific backbone assignment of the protein (or proteins) under investigation, we next determined the sequence-specific backbone assignment of the RBD. The fully annotated 2D [^{1}H,^{15}N] TROSY-spectrum of the RBD is shown in Figure 1B. The completeness of the sequence-specific backbone assignments of the expected backbone peaks is 88% (166/186). Most residues in functionally critical regions, including the major RBD epitopes, are assigned, with the assignments for the RBS, CR3022, and S309 binding sites being 86%, 79%, and 89% complete, respectively. Unassigned RBD residues are largely localized to a single patch near the RBD N-terminus, which overlaps just slightly with the bottom tips of the CR3022 and S309 binding surfaces (Figure 1C). Chemical shift index calculations derived from Cα and Cβ chemical shifts showed that the secondary structure elements of the RBD in solution map perfectly to those observed in the RBD crystal structure (Figure 1D; compared to RBD crystal structure in PDBID 6W41[11]).

The dynamics of the RBD domain were analyzed using ^{15}N{^{1}H}-NOE (hetNOE) measurements, which reports on fast time scale (ps to ns) backbone motions. Three regions in the RBD have residues with hetNOE values <0.7:368−375 loop, 382−387 loop, and 476−489 loop, indicating higher flexibility. Consistent with this result, these loops exhibit higher variability in crystal structures of the RBD (for resolutions better than 2.25 Å). While loops 368−375 and 382−387 directly flank the CR3022 binding interface, loop 476−489 defines the ridge bound by the ACE2 receptor and many RBS mAbs (Figure 2A−C).

Next we asked if CSP mapping would be a viable approach for identifying Fab:RBD interaction surfaces. For this proof-of-principle study, we used the Fab from the well-characterized mAb CR3022 (hereafter, the Fab is referred to as CR3022).[18] CR3022 was derived from a mAb that was originally isolated from a SARS-CoV convalescent patient.[19] It was later shown to

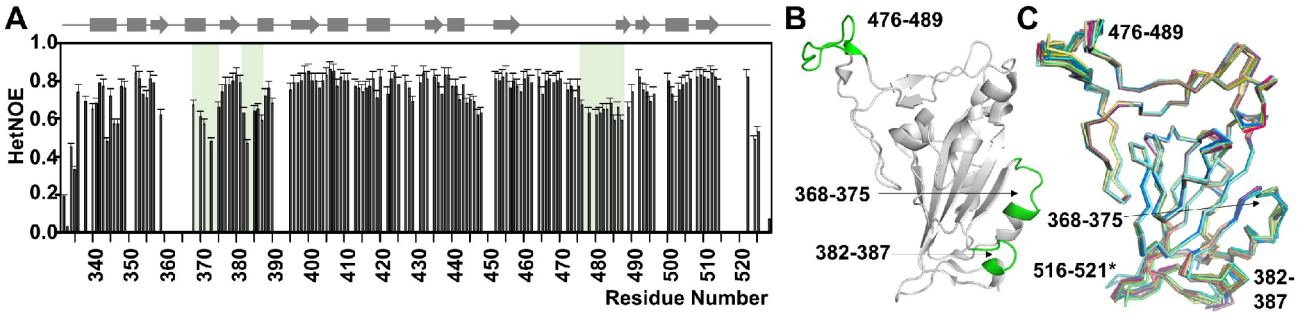

Figure 2. RBD dynamics. (A) ^{15}N{^{1}H}-NOE of the RBD (600 MHz ^{1}H Larmor) identifies three loops with increased flexibility (light green background: 368−375, 382−387, and 476−489). (B) Cartoon of the RBD with the three flexible loops colored green; RBD orientation identical to that in Figure 1A, left panel. (C) Overlay of RBD crystal structures with the RBD from 6w41 (2.25 Å resolution or better: 7EAN, 7KFY, 7KFX, 7LM8, 7CJF, 7DEU, 7KN5[23], 7KMI, 7LOP, 7B3O, 6YZ5, 7EAM; average Cα−Cα RMSD is 0.91 Å, 1.18 Å, 0.89 Å, and 1.07 Å for loops 368−375, 382−387, 476−489, and 516−521, respectively; overall Cα−Cα RMSD is 0.51 Å). Residues 516−521 (*) are unassigned.

https://doi.org/10.1021/jacs.1c03945
J. Am. Chem. Soc. 2021, 143, 7930−7934

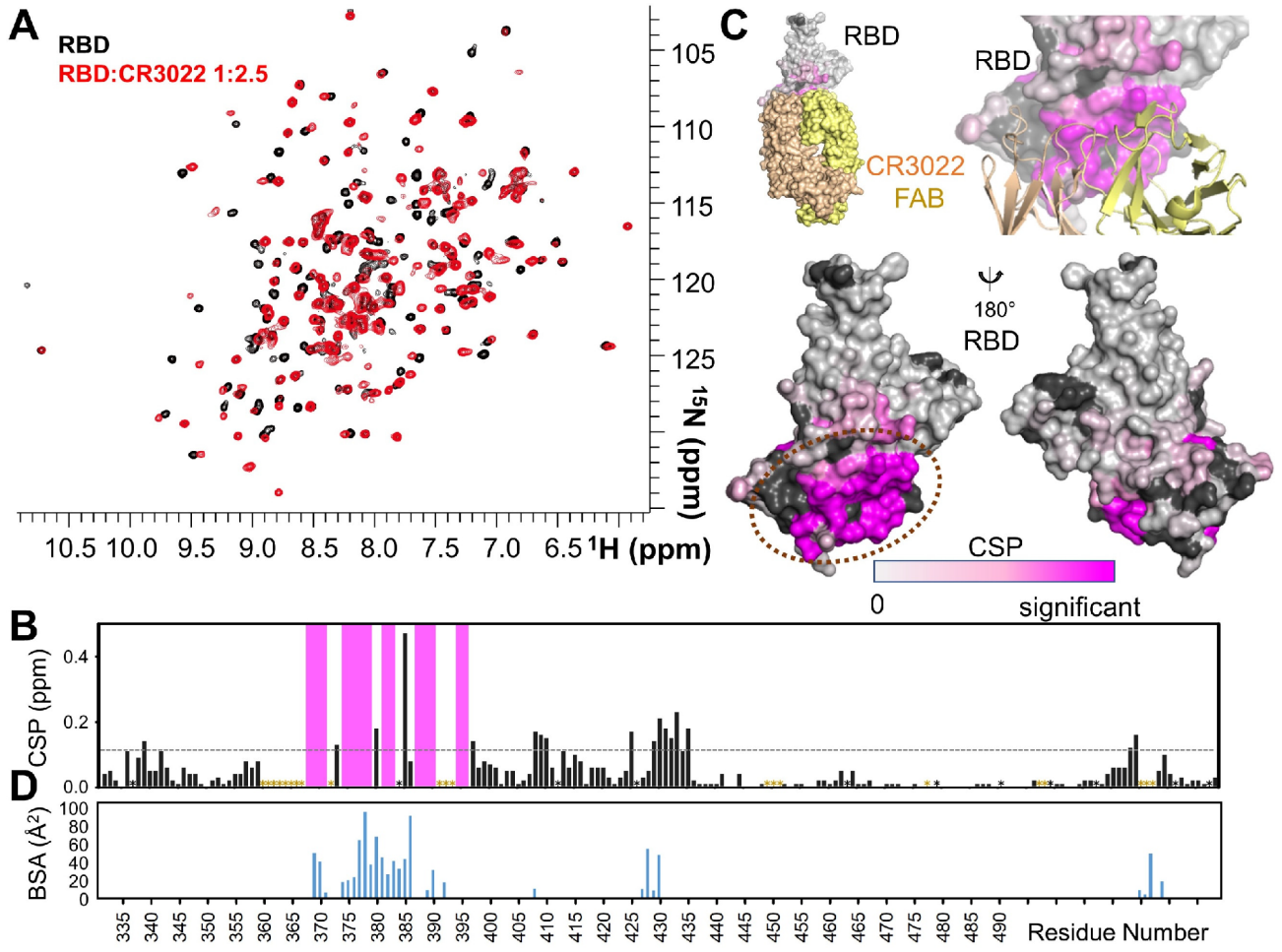

Figure 3. CSP mapping identifies RBD epitopes. (A) Overlay of the 2D [^{1}H,^{15}N] TROSY spectrum of the (^{2}H,^{15}N)-labeled SARS-CoV-2 RBD in the absence (black) and presence (red; 1:2.5 molar ratio; saturation was reached at a 1:1 molar ratio but the 1:2.5 spectrum, which is shown, has the best S/N ratio due increased recording time) of CR3022 (800 MHz ^{1}H Larmor). (B) CSPs of RBD in the presence of CR3022. Pro residues and residues missing backbone assignment are shown as '*' (black, Pro; yellow, unassigned). The 20 residues that shifted to an extent that they could not be confidently assigned by analyzing nearest peak are shown as pink bars. Nineteen residues exhibit CSPs greater than 2σ (0.12 ppm, gray dashed line). (C) RBD CSPs mapped onto the RBD surface with extent of CSP indicated by color (light gray, no observed CSP, to magenta, most significant CSPs). *Upper*, RBD with the CR3022 Fab heavy (yellow) and light (beige) chains shown as either a surface or a cartoon; *lower*, RBD with CSPs mapped onto the surface (proline/unassigned residues in black). Dashed orange ellipse indicates major CR3022 Fab binding interface. (D) Buried solvent accessible surface area (BSA, buried surface area) of RBD residues when bound to CR3022 (PDBID 6W41).

cross-react with the RBD from SARS-CoV-2.[20] Because the structure of CR3022 bound to the SARS-CoV-2 RBD has been determined using X-ray crystallography,[11] the overlap between the interface determined using NMR chemical shift perturbation mapping and X-ray crystallography can be readily assessed.

In this experiment, (^{2}H,^{15}N)-labeled RBD was incubated with increasing ratios of unlabeled CR3022 (1:1.1, 1:2, 1:2.5) and a 2D [^{1}H,^{15}N] TROSY spectrum recorded. The spectrum is of excellent quality for a complex of this size (70 kDa) with no apparent loss of signals due to line broadening and the ^{1}H,^{15}N cross-peaks are well-resolved (Figure 3A). Thus, the chemical shift perturbations in the RBD caused by CR3022 binding can be readily detected. Direct comparison of the 2D [^{1}H,^{15}N] TROSY spectra of the free and CR3022-bound RBD revealed CSPs, which allowed 145 peaks to be readily assigned, 19 of which experience CSPs greater than 2σ (Figure 3B). The remaining ~20 peaks shifted to such a great extent that they could not be confidently assigned. Mapping the residues that experience CSPs onto the surface of the RBD shows that the majority of the most significantly shifted peaks correspond to residues at the RBD-CR3022 interface (Figure 3C, D). In particular, comparing the residue-specific CSPs with the corresponding buried solvent accessible surface area shows that the major and two minor interaction sites (major: residues 369−392; minor: residues 427−430, 515−519) as identified using X-ray crystallography (Figure 3D) are also readily identified using NMR CSP mapping (Figure 3B), with the major interaction site residues, which constitute 78% of the total RBD BSA, corresponding to those residues that experience the largest CSPs. Further, of the 29 residues that constitute the CR3022 interface, 26 experience a CSP that is either greater than the 2σ threshold or shifted to such an extent they could not be confidently assigned (only K386, D427, and D428 had CSPs less than the 2σ threshold). These data unequivocally confirm that CSP mapping is an ideal approach for rapidly identifying the RBD residues that bind RBD-specific Fabs.

The data also show that there are also some small differences between the two techniques. For example, K386 experiences

https://doi.org/10.1021/jacs.1c03945
J. Am. Chem. Soc. 2021, 143, 7930−7934

the second largest loss of solvent accessible surface area upon CR3022 binding, while its CSP is less than the 2σ threshold. This is because CR3022 binding fully buries the K386 side chain, which results in a large loss of solvent accessible surface area, while the CSP measure changes in the amide-proton backbone. Together, these results demonstrate that, for K386, CR3022 interacts predominantly with the side chain versus the backbone. Conversely, three residues (408−410) experience CSPs greater than the 2σ threshold, yet only one of these residues, R408, has solvent accessible surface area buried by CR3022 and the extent is only minimal (10 Å^2; side chain). Although the R408 BSA change is minimal, the CSP data demonstrate that this residue defines a minor interaction site. Thus, NMR CSP mapping, in addition to identifying major binding epitopes, also readily identifies minor interaction sites.

Together, these data demonstrate that current ambitious efforts to correlate RBD-specific mAb binding mechanisms with neutralization efficacy can be greatly accelerated by incorporating NMR CSP mapping, in addition to X-ray crystallography and cryo-EM, for characterizing the Fab-RBD interface at molecular resolution. Although using CSP mapping for identifying Fab-antigen interfaces is not new,[21,22] it has not been widely used, likely due in part to the need for an antigen that is amenable for NMR spectroscopy. Here, we show that the RBD domain is ideal for these studies and that CSP mapping will allow the full complement of RBD-mAb to be rapidly defined. Because NMR readily detects interactions with even mM affinities, any reduction in affinity due to the absence of glycosylation on RBD residue N343 is not expected to negatively impact epitope identification. Finally, by generating variants of the RBD that are present in novel, more infectious SARS-CoV-2 strains, one can also use CSP mapping to identify, at a molecular level, how the Fab-RBD interaction changes as a result of RBD mutations. Together, by integrating biomolecular liquid-state NMR with X-ray crystallography and cryo-EM for defining all RBD-Fab interactions and correlating these data with neutralization efficacy, structure-based approaches. for the development of improved vaccines and COVID-19 mAb-based therapies may be more rapidly realized.

■ ASSOCIATED CONTENT

Supporting Information

The Supporting Information is available free of charge at https://pubs.acs.org/doi/10.1021/jacs.1c03945.

Experimental protocols and supplemental figures (PDF)

■ AUTHOR INFORMATION

Corresponding Authors

Wolfgang Peti − *Department of Molecular Biology and Biophysics, University of Connecticut Health Center, Farmington, Connecticut 06030, United States;* orcid.org/0000-0002-8830-6594; Email: peti@uchc.edu

Rebecca Page − *Department of Cell Biology, University of Connecticut Health Center, Farmington, Connecticut 06030, United States;* orcid.org/0000-0002-4645-1232; Email: rpage@uchc.edu

Authors

Marta V. Schoenle − *Biochemistry Graduate Program, University of Arizona, Tucson, Arizona 85721, United States;* Present Address: Department of Immunobiology, University of Arizona, Tucson, Arizona, 85721, USA.

Yang Li − *Department of Molecular Biology and Biophysics, University of Connecticut Health Center, Farmington, Connecticut 06030, United States*

Meng Yuan − *Department of Integrative Structural and Computational Biology, The Scripps Research Institute, La Jolla, California 92037, United States*

Michael W. Clarkson − *Deparment of Chemistry and Biochemistry, University of Arizona, Tucson, Arizona 85721, United States*

Ian A. Wilson − *Department of Integrative Structural and Computational Biology, The Scripps Research Institute, La Jolla, California 92037, United States; The Skaggs Institute for Chemical Biology, The Scripps Research Institute, La Jolla, California 92037, United States*

Complete contact information is available at: https://pubs.acs.org/10.1021/jacs.1c03945

Notes

The authors declare no competing financial interest.

The BMRB accession number for SARS-CoV-2 RBD assignment is 50809.

■ ACKNOWLEDGMENTS

This work was supported in part by the Bill and Melinda Gates Foundation OPP1170236 and INV-004923 (I.A.W.) and University of Connecticut Health Center start-up funds (R.P., W.P.).

■ REFERENCES

(1) Polack, F. P.; Thomas, S. J.; Kitchin, N.; Absalon, J.; Gurtman, A.; Lockhart, S.; Perez, J. L.; Pérez Marc, G.; Moreira, E. D.; Zerbini, C.; Bailey, R.; Swanson, K. A.; Roychoudhury, S.; Koury, K.; Li, P.; Kalina, W. V.; Cooper, D.; Frenck, R. W.; Hammitt, L. L.; Türeci, Ö.; Nell, H.; Schaefer, A.; Ünal, S.; Tresnan, D. B.; Mather, S.; Dormitzer, P. R.; Şahin, U.; Jansen, K. U.; Gruber, W. C. C4591001 Clinical Trial Group. Safety and Efficacy of the BNT162b2MRNA Covid-19 Vaccine. *N. Engl. J. Med.* **2020**, *383* (27), 2603−2615.

(2) Tegally, H.; Wilkinson, E.; Giovanetti, M.; Iranzadeh, A.; Fonseca, V.; Giandhari, J.; Doolabh, D.; Pillay, S.; San, E. J.; Msomi, N.; Mlisana, K.; von Gottberg, A.; Walaza, S.; Allam, M.; Ismail, A.; Mohale, T.; Glass, A. J.; Engelbrecht, S.; Van Zyl, G.; Preiser, W.; Petruccione, F.; Sigal, A.; Hardie, D.; Marais, G.; Hsiao, N.-Y.; Korsman, S.; Davies, M.-A.; Tyers, L.; Mudau, I.; York, D.; Maslo, C.; Goedhals, D.; Abrahams, S.; Laguda-Akingba, O.; Alisoltani-Dehkordi, A.; Godzik, A.; Wibmer, C. K.; Sewell, B. T.; Lourenço, J.; Alcantara, L. C. J.; Kosakovsky Pond, S. L.; Weaver, S.; Martin, D.; Lessells, R. J.; Bhiman, J. N.; Williamson, C.; de Oliveira, T. Detection of a SARS-CoV-2 Variant of Concern in South Africa. *Nature* **2021**, *592* (7854), 438−443.

(3) Greaney, A. J.; Starr, T. N.; Gilchuk, P.; Zost, S. J.; Binshtein, E.; Loes, A. N.; Hilton, S. K.; Huddleston, J.; Eguia, R.; Crawford, K. H. D.; Dingens, A. S.; Nargi, R. S.; Sutton, R. E.; Suryadevara, N.; Rothlauf, P. W.; Liu, Z.; Whelan, S. P. J.; Carnahan, R. H.; Crowe, J. E.; Bloom, J. D. Complete Mapping of Mutations to the SARS-CoV-2 Spike Receptor-Binding Domain That Escape Antibody Recognition. *Cell Host Microbe* **2021**, *29* (1), 44−57.e9.

(4) Collier, D. A.; De Marco, A.; Ferreira, I. A. T. M.; Meng, B.; Datir, R. P.; Walls, A. C.; Kemp, S. A.; Bassi, J.; Pinto, D.; Silacci-Fregni, C.; Bianchi, S.; Tortorici, M. A.; Bowen, J.; Culap, K.; Jaconi, S.; Cameroni, E.; Snell, G.; Pizzuto, M. S.; Pellanda, A. F.; Garzoni, C.; Riva, A.; CITIID-NIHR BioResource COVID-19 Collaboration; Elmer, A.; Kingston, N.; Graves, B.; McCoy, L. E.; Smith, K. G. C.; Bradley, J. R.; Temperton, N.; Ceron-Gutierrez, L.; Barcenas-Morales, G.; COVID-19 Genomics UK (COG-UK) Consortium; Harvey, W.; Virgin, H. W.; Lanzavecchia, A.; Piccoli, L.; Doffinger, R.; Wills, M.; Veesler, D.; Corti, D.; Gupta, R. K. Sensitivity of SARS-CoV-2 B.1.1.7

to mRNA Vaccine-Elicited Antibodies. *Nature* **2021**, *593* (7857), 136−141.
(5) Walls, A. C.; Park, Y.-J.; Tortorici, M. A.; Wall, A.; McGuire, A. T.; Veesler, D. Structure, Function, and Antigenicity of the SARS-CoV-2 Spike Glycoprotein. *Cell* **2020**, *183* (6), 1735.
(6) McCallum, M.; De Marco, A.; Lempp, F. A.; Tortorici, M. A.; Pinto, D.; Walls, A. C.; Beltramello, M.; Chen, A.; Liu, Z.; Zatta, F.; Zepeda, S.; di Iulio, J.; Bowen, J. E.; Montiel-Ruiz, M.; Zhou, J.; Rosen, L. E.; Bianchi, S.; Guarino, B.; Fregni, C. S.; Abdelnabi, R.; Foo, S.-Y. C.; Rothlauf, P. W.; Bloyet, L.-M.; Benigni, F.; Cameroni, E.; Neyts, J.; Riva, A.; Snell, G.; Telenti, A.; Whelan, S. P. J.; Virgin, H. W.; Corti, D.; Pizzuto, M. S.; Veesler, D. N-Terminal Domain Antigenic Mapping Reveals a Site of Vulnerability for SARS-CoV-2. *Cell* **2021**, *184* (9), 2332−2347.e16.
(7) Turoňová, B.; Sikora, M.; Schürmann, C.; Hagen, W. J. H.; Welsch, S.; Blanc, F. E. C.; von Bülow, S.; Gecht, M.; Bagola, K.; Hörner, C.; van Zandbergen, G.; Landry, J.; de Azevedo, N. T. D.; Mosalaganti, S.; Schwarz, A.; Covino, R.; Mühlebach, M. D.; Hummer, G.; Krijnse Locker, J.; Beck, M. In Situ Structural Analysis of SARS-CoV-2 Spike Reveals Flexibility Mediated by Three Hinges. *Science* **2020**, *370* (6513), 203−208.
(8) Hoffmann, M.; Kleine-Weber, H.; Schroeder, S.; Krüger, N.; Herrler, T.; Erichsen, S.; Schiergens, T. S.; Herrler, G.; Wu, N.-H.; Nitsche, A.; Müller, M. A.; Drosten, C.; Pöhlmann, S. SARS-CoV-2 Cell Entry Depends on ACE2 and TMPRSS2 and Is Blocked by a Clinically Proven Protease Inhibitor. *Cell* **2020**, *181* (2), 271−280.e8.
(9) Wang, Q.; Zhang, Y.; Wu, L.; Niu, S.; Song, C.; Zhang, Z.; Lu, G.; Qiao, C.; Hu, Y.; Yuen, K.-Y.; Wang, Q.; Zhou, H.; Yan, J.; Qi, J. Structural and Functional Basis of SARS-CoV-2 Entry by Using Human ACE2. *Cell* **2020**, *181* (4), 894−904.e9.
(10) Raybould, M. I. J.; Kovaltsuk, A.; Marks, C.; Deane, C. M. CoV-AbDab: The Coronavirus Antibody Database. *Bioinformatics* **2021**, *37* (5), 734−735.
(11) Yuan, M.; Wu, N. C.; Zhu, X.; Lee, C.-C. D.; So, R. T. Y.; Lv, H.; Mok, C. K. P.; Wilson, I. A. A Highly Conserved Cryptic Epitope in the Receptor Binding Domains of SARS-CoV-2 and SARS-CoV. *Science* **2020**, *368* (6491), 630−633.
(12) Yuan, M.; Liu, H.; Wu, N. C.; Wilson, I. A. Recognition of the SARS-CoV-2 Receptor Binding Domain by Neutralizing Antibodies. *Biochem. Biophys. Res. Commun.* **2021**, *538*, 192−203.
(13) Yuan, M.; Liu, H.; Wu, N. C.; Lee, C.-C. D.; Zhu, X.; Zhao, F.; Huang, D.; Yu, W.; Hua, Y.; Tien, H.; Rogers, T. F.; Landais, E.; Sok, D.; Jardine, J. G.; Burton, D. R.; Wilson, I. A. Structural Basis of a Shared Antibody Response to SARS-CoV-2. *Science* **2020**, *369* (6507), 1119−1123.
(14) Lv, H.; Wu, N. C.; Tsang, O. T.-Y.; Yuan, M.; Perera, R. A. P. M.; Leung, W. S.; So, R. T. Y.; Chan, J. M. C.; Yip, G. K.; Chik, T. S. H.; Wang, Y.; Choi, C. Y. C.; Lin, Y.; Ng, W. W.; Zhao, J.; Poon, L. L. M.; Peiris, J. S. M.; Wilson, I. A.; Mok, C. K. P. Cross-Reactive Antibody Response between SARS-CoV-2 and SARS-CoV Infections. *Cell Rep.* **2020**, *31* (9), 107725.
(15) Barnes, C. O.; Jette, C. A.; Abernathy, M. E.; Dam, K.-M. A.; Esswein, S. R.; Gristick, H. B.; Malyutin, A. G.; Sharaf, N. G.; Huey-Tubman, K. E.; Lee, Y. E.; Robbiani, D. F.; Nussenzweig, M. C.; West, A. P.; Bjorkman, P. J. SARS-CoV-2 Neutralizing Antibody Structures Inform Therapeutic Strategies. *Nature* **2020**, *588* (7839), 682−687.
(16) Yuan, M.; Huang, D.; Lee, C.-C. D.; Wu, N. C.; Jackson, A. M.; Zhu, X.; Liu, H.; Peng, L.; van Gils, M. J.; Sanders, R. W.; Burton, D. R.; Reincke, S. M.; Prüss, H.; Kreye, J.; Nemazee, D.; Ward, A. B.; Wilson, I. A. Structural and Functional Ramifications of Antigenic Drift in Recent SARS-CoV-2 Variants. **02/17/2021**. *bioRxiv* DOI: 10.1101/2021.02.16.430500 (accessed 05/12/2021).
(17) Pervushin, K.; Riek, R.; Wider, G.; Wüthrich, K. Attenuated T2 Relaxation by Mutual Cancellation of Dipole-Dipole Coupling and Chemical Shift Anisotropy Indicates an Avenue to NMR Structures of Very Large Biological Macromolecules in Solution. *Proc. Natl. Acad. Sci. U. S. A.* **1997**, *94* (23), 12366−12371.
(18) Hussain, A.; Hasan, A.; Nejadi Babadaei, M. M.; Bloukh, S. H.; Chowdhury, M. E. H.; Sharifi, M.; Haghighat, S.; Falahati, M. Targeting SARS-CoV2 Spike Protein Receptor Binding Domain by Therapeutic Antibodies. *Biomed. Pharmacother.* **2020**, *130*, 110559.
(19) ter Meulen, J.; van den Brink, E. N.; Poon, L. L. M.; Marissen, W. E.; Leung, C. S. W.; Cox, F.; Cheung, C. Y.; Bakker, A. Q.; Bogaards, J. A.; van Deventer, E.; Preiser, W.; Doerr, H. W.; Chow, V. T.; de Kruif, J.; Peiris, J. S. M.; Goudsmit, J. Human Monoclonal Antibody Combination against SARS Coronavirus: Synergy and Coverage of Escape Mutants. *PLoS Med.* **2006**, *3* (7), No. e237.
(20) Tian, X.; Li, C.; Huang, A.; Xia, S.; Lu, S.; Shi, Z.; Lu, L.; Jiang, S.; Yang, Z.; Wu, Y.; Ying, T. Potent Binding of 2019 Novel Coronavirus Spike Protein by a SARS Coronavirus-Specific Human Monoclonal Antibody. *Emerging Microbes Infect.* **2020**, *9* (1), 382−385.
(21) Morgan, W. D.; Lock, M. J.; Frenkiel, T. A.; Grainger, M.; Holder, A. A. Malaria Parasite-Inhibitory Antibody Epitopes on *Plasmodium Falciparum* Merozoite Surface Protein-1(19) Mapped by TROSY NMR. *Mol. Biochem. Parasitol.* **2004**, *138* (1), 29−36.
(22) Blech, M.; Seeliger, D.; Kistler, B.; Bauer, M. M. T.; Hafner, M.; Hörer, S.; Zeeb, M.; Nar, H.; Park, J. E. Molecular Structure of Human GM-CSF in Complex with a Disease-Associated Anti-Human GM-CSF Autoantibody and Its Potential Biological Implications. *Biochem. J.* **2012**, *447* (2), 205−215.

https://doi.org/10.1021/jacs.1c03945
J. Am. Chem. Soc. 2021, 143, 7930−7934